PHYSICAL REVIEW E **73**, 055701(R) (2006)

Simulation of a microfluidic flow-focusing device

Michael M. Dupin
Steele Laboratory, Massachusetts General Hospital and Harvard Medical School, Boston, Massachusetts 02114, USA

Ian Halliday and Chris M. Care
Materials and Engineering Research Institute, Sheffield Hallam University, Sheffield S1 1WB, United Kingdom

(Received 8 April 2005; published 17 May 2006)

We present a model of microfluidic flow of several completely immiscible fluids and use it to simulate a whole flow focusing device chamber. Our efficient, practical model supports a large parameter space, spanned by surface wetting, surface tension, liquid-liquid wetting, viscosity ratio, and inlet velocity. It is based upon an N-component lattice Boltzmann method with interrupted coalescence [Dupin *et al.*, Philos. Trans. R. Soc. London, Ser. A **362**, 1885 (2004)], here adapted for calculations at low capillary and Reynolds numbers, with wetting and significantly reduced spurious flow. Results over 2 orders of magnitude in Reynolds number are presented.

DOI: 10.1103/PhysRevE.73.055701 PACS number(s): 47.11.Qr, 47.15.G−

I. INTRODUCTION

Recently there has been interest in microscale apparatuses containing two immiscible liquids, designed to form uniform droplets e.g., [1,2], which produce colloids of unprecedented uniformity and so may form the basis of a *lab-on-a-chip*. Anna's "flow-focusing" geometry [1] is shown in Fig. 1. Its flow, classified as continuum-scale, unsteady, and interface-dominated, is characterized by a low drop Reynolds number, Re_d, and a low to intermediate capillary number, Ca. The modeling problem is compounded by liquid-liquid and liquid-solid wetting.

Simulating Anna's device by traditional computation fluid dynamics (CFD) is computationally expensive, partially due to interface tracking costs. Another challenge is the combination of low Re_d and Ca, which means that spurious velocities (present in most computational schemes) compare in magnitude to the modeled flow velocity. We report results obtained by a lattice Boltzmann (LB) method. LB methods for fluid flows have developed since the late 1980s [3,4]; for a recent, comprehensive, survey see [5]; the particular variant we use synthesizes and enhances Dupin and co-workers' [6] multicomponent LB model and co-workers' [7] and Lishchuk's LB model. A less refined version of our method has been successfully applied to venule-scale blood flow [6,8]. We note in passing, the recent advent of microfluidic-adapted LB methods [9,10] (containing, e.g., electrostatic interactions and boundary slip), some of which have achieved some success [11–13]. However, at the present scale, a traditional LB fluid model is equally valid; see Sec. II. Several multicomponent LB versions are distinguished by the particular way in which the fluid-fluid interface is imposed (e.g., [7,14–16]). The method of Swift *et al.* [14], based on the Cahn-Hilliard theory, is an appropriate choice when phase separation kinematics feature. However, in our application, the continuum approximation (small Knudsen number) and a consistency across length scales urge a model with narrow interfaces and a continuum model of wetting.

In this work, we combine existing LB methods in context *before* defining the necessary model enhancements. In so doing, we emphasize the significance of the latter. Accordingly, this article is organized as follows. Section II outlines background detail of our LB model, Sec. III considers the key combinations of particular LB model components in a flow-focusing context, Sec. IV describes model extensions, and Secs. V and VI contain results and conclusions.

II. BACKGROUND LATTICE BOLTZMANN MODEL

Our particular multiple immiscible component LB model [6,8,17] is based on the single component Bhatnagar-Gross-Krook (LBGK) version [18] with a source term $\phi_i(\mathbf{r})$ [5] added for interfacial tension:

$$f_i(\mathbf{r}+\mathbf{c}_i,t+1) = f_i(\mathbf{r},t) - \frac{1}{\tau}(f_i(\mathbf{r},t) - f_i^0(\rho,\rho\mathbf{u})) + \phi_i(\mathbf{r}), \qquad (1)$$

velocity vectors, $\mathbf{c}_i$, being the $D2Q9$ set [5]. Essentially, immiscible fluid component C is tracked using phase field, ρ_M^C, at boundaries in which ϕ_i generates a body force [7] for interfacial tension. Optimally sharp interfaces arise by a numerical segregation process [15] (below), so our model maintains (within numerical error) a complete, mutual, segregation of all components with all coalescence interrupted; it contains no phase separation kinematics in the same way as Swift and colleagues' method [14].

Dupin and co-workers' [6,18] multicomponent LB model decomposes the single momentum density, f_i, into a set of $N_C(\mathbf{r},t)$ contributions, $f_i^C(\mathbf{r},t)$, such that:

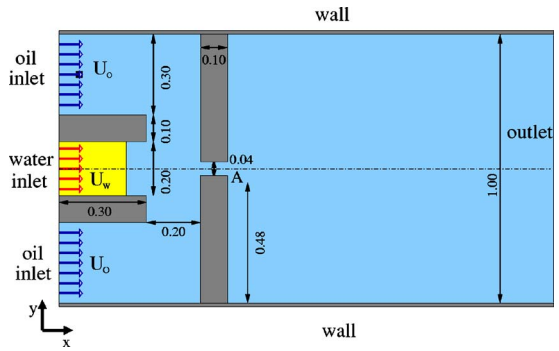

FIG. 1. (Color online) Schematic of a flow focusing geometry, e.g., [1].

$$f_i(\mathbf{r},t) = \sum_C f_i^C(\mathbf{r},t), \tag{2}$$

where the f_i evolve according to Eq. (1) and the value of superscript C runs over the $N_C(\mathbf{r},t)$ components present locally. Density, $\rho(\mathbf{r},t)$, is likewise decomposed into partial contributions from each local component:

$$\rho(\mathbf{r},t) = \sum_C \left(\rho^C(\mathbf{r},t) = \sum_i f_i^C(\mathbf{r},t)\right), \tag{3}$$

with fluid velocity: $\rho(\mathbf{r},t)\mathbf{u}(\mathbf{r},t) = \sum_i f_i(\mathbf{r},t)\mathbf{c}_i$. To segregate different components, define a phase index:

$$\rho_M^C(\mathbf{r},t) \equiv 1 - 2\frac{\rho^C(\mathbf{r},t)}{\rho(\mathbf{r},t)}; \quad -1 \leqslant \rho_M^C(\mathbf{r},t) \leqslant 1. \tag{4}$$

C superscripts (i.e., f_i^Cs) are reset "numerically," [15] at *mixed* nodes $|\rho_M^C(\mathbf{r},t)| < 0.99$ after a collision. Component C, present in amount ρ^C, is allocated hierarchically, beginning at the f_i with that velocity, $\mathbf{c}_i$, of largest projection on its color field:

$$\widehat{\mathbf{G}^C} \equiv \nabla\rho_M^C(\mathbf{r},t) = 3\sum_i t_p\rho^C(\mathbf{r}+\mathbf{c}_i,t)\mathbf{c}_i + O((c)_i^3). \tag{5}$$

This maximizes the flux of C, $\mathbf{q}^C$, in $\widehat{\mathbf{G}^C}$ and generates a narrow interface, some 1.5 lattice spacings across. On recognizing that sharp interfaces mean $N_C(\mathbf{r},t) \leqslant 5$ may be assumed locally (the number of different components globally, N, being unlimited) there results a computationally efficient method for simulating a large number of immiscible species [6,8]. Only five discrete values of C and 5 (sets of) momentum distribution functions are required at each site, so memory and computing time are virtually independent of N and the distribution of fluid components.

At a mixed node, interfacial tension is applied for each C by a generalized form of Lishchuk and co-workers' perturbation for a body force at the Navier-Stokes scale, proportional in strength to the local interface curvature $K^C(\mathbf{r},t)$:

$$\mathbf{F}^C(\mathbf{r},t) = \frac{3}{2}K^C(\mathbf{r},t)\sigma^C\rho^C(\mathbf{r},t), \tag{6}$$

where $K^C(\mathbf{r},t)$ is obtained from the second derivatives of $\nabla\rho^C$ [7]. Generalizing the analysis of [7], the source term to generate a macroscopic, body force for all the interfaces present locally is

$$\phi_i(\mathbf{r},t) = \frac{3}{2}\sum_C \left(\sigma^C K^C(\mathbf{r},t)c_{i\beta}\frac{\partial}{\partial x_\beta}\rho_M^C(\mathbf{r},t)\right). \tag{7}$$

For two fluids, C and D, Eq. (7) becomes $\phi_i(\mathbf{r},t) = \frac{3}{2}(\sigma^C + \sigma^D)K^C(\mathbf{r},t)c_{i\beta}\frac{\partial}{\partial x_\beta}\rho_M^C(\mathbf{r},t)$, giving the macroscopic interfacial tension $\sigma^C + \sigma^D$ [7].

III. APPLICATION TO FLOW FOCUSING

In the experiments of Anna *et al.* [1] (Fig. 1), distilled water, viscosity ν_W, and silicon oil, viscosity $\nu_O = 6\nu_W$, enter as indicated. Forced into a narrow thread, the water breaks into uniform drops upstream or downstream of A, according to parametrization. Drop size depends on inlet velocities. Surfactant dissolved in the oil interrupts water drops' coalescence. This apparatus will be considered as a pressure-driven flow with open boundary conditions.

For the current application (see Fig. 1), we estimate the Reynolds number $\mathrm{Re} \equiv U_O W_O/\nu_O \gtrsim 10^{-1}$ and the capillary number $\mathrm{Ca} \equiv \nu_O|U_O - U_W|/\alpha \gtrsim 10^{-4}$ (where α is the interfacial macroscopic surface tension). It must be noted here that this flow regime is particularly difficult to address with common computational methods (mainly due to the emergence of unwanted spurious flow, see Sec. IV). Flow in the geometry of Fig. 1 is influenced by the two fluids' dynamic contact line (DCL) behavior at the solid boundaries. The continuum description breaks down close to a DCL and, strictly, one should resolve the interface structure. However, one can use one of several continuum approximation strategies; here we choose to use a form of the Navier boundary condition [19].

Perhaps the most important, existing property of our model outlined in Sec. II is its control of coalescence. The input oil stream and the stabilized drops are represented as mutually immiscible liquids with the same physical properties. We detect oil drop scission by monitoring the phase field, ρ^O, representing the oil profile, along the central axis of the simulation. The separation of a drop is identified as the appearance of a zero in the profile and the fluid in the droplet is relabeled to a new, unique, value. Different liquids, albeit with identical properties, are treated as immiscible by default in Dupin's algorithm. Note while this creates a new liquid component in the simulation, it leaves the total data storage requirement, unchanged. Also note that execution speed is only slightly reduced as additional interface appears.

In the case of three or more liquids at a node, the water fluid was made preferentially to wet by setting its parameter $\sigma^W < 0$ [Eq. (6)] and setting $G^C \to -G^C$ locally; all interfacial tensions of course remain positive [see note after Eq. (7)], but with three fluids in contact, this device encourages a thin layer of water to prevent the close approach between drops, circumventing a need to postulate sublattice lubrication forces.

Open boundary conditions are present on the left and right faces of Fig. 1. Inlet and outlet fluxes and an outlet pressure (density) distribution were specified at every time step, using an appropriate equilibrium $f_i^{(0)}(\rho,\mathbf{u})$ [5]. The inlet pressure distribution was allowed to develop. The inlet fluxes are indicated in Fig. 1; the corresponding outlet flux was taken to be a square profile of matched discharge. The unknown inlet density developed using a "fully developed," uniform pressure gradient condition [17]. No-slip walls were applied by the robust method of midlink bounceback [5], which, while only 0(1.5) accurate, conveniently resolves our complex wall shapes. Wetting at these walls is discussed in Sec. IV.

To support the large axial pressure gradient about orifice A (Fig. 1), it was necessary to use an exactly incompressible (EI) form of the LBGK method [shortened as exactly incompressible Bhatnagar-Gross-Krook (EILBGK)]. He and Luo's [20] D2Q9 EILBGK scheme was used for the overall fluid. In this method, the average LB fluid density is assumed constant, locally the pressure $P = \rho$ and the effect of LB fluid compressibility, originating in LB's $O(1)$ speed of sound, is removed. Errors associated with the time variation in EILBGK schemes were measured as negligible in the slow flow of this configuration.

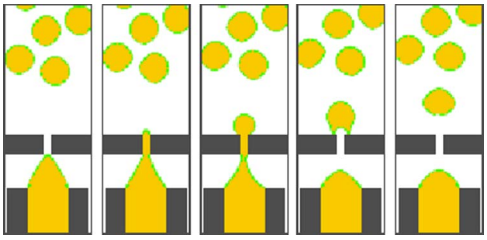

FIG. 2. (Color online) Detail of the velocity field of simulation in Fig. 3(a), showing a clean velocity field. Paired vortices are consistent with the experimental counterpart.

IV. ENHANCED MULTICOMPONENT LATTICE BOLTZMANN

A. Phase fields at the wall

To control wetting one must control the direction of the color flux at the wall. Consider mixed nodes on a no-slip boundary; steps (i) and (ii) below reduce spurious flow by more than an order of magnitude. (i) Segregating liquids "symmetrically" when $\nabla\rho_M^C$ lies within ±5° of a lattice link direction. Numerical species segregation generates sharp interfaces by preferentially populating links with the largest projection on $\nabla\rho_M^C$ with color C. However, this gives a flux of color C, which fluctuates about the direction of $\nabla\rho_M^C$, the instantaneous direction of the flux of C only approximating that of $\nabla\rho_M^C$. It is essential to correlate the directions of $\nabla\rho_M^C$ and the C flux for nodes lying close to a wall. For our application, no-slip walls were placed parallel to lattice directions. To allow the C flux to resolve the wall orientation, subsets of the three LB lattice links with the largest projection on $\nabla\rho_M^C$ had equal priority for the allocation of color C. The value of 5° is based on trial and error. Decreasing this angle limits the benefits of equal recoloring while increasing it decreases efficiency. (ii) Systematic error in the boundary-normal component of $\nabla\rho_M^C$ leads to errors in the emergent DCL behavior through the misdirection of the flux of ρ_M^C [17]. Therefore, we calculated the boundary value of $\nabla\rho_M^C$ at a point displaced by 0.5 lattice spacings along the wet boundary normal.

B. Contact line motion

Dynamic contact lines (DCLs) are an open question. To avoid a singularity, we assume a subgrid layer of supernatant wets the walls and that wetting in low-inertia flow is dominated by competition between fluids' postulated wetting affinities. Interfacial slip in the DCL region is assumed to be determined by an uncompensated Young stress alone, as follows. Let $\hat{T}$ denote the boundary tangent. Suppose components C and C' are present. A "boundary body force" parametrized by σ_W^C, determines the wetting affinity of component C: $F_b^C = \sigma_W^C |(\hat{T}\nabla)\rho_C^N|$. It acts parallel to the walls, into fluid C [17]. Corresponding similar forces are applied to all fluids of the mixture present in contact with the wall. Wetting of a given CC' interface is the combination of each wetting affinity for the pair constituents C and C'.

C. Stability and parameter range

The range of modelled behavior is controlled by (i) the boundary conditions, especially the magnitude of the pressure gradient and (ii) the range of Ca between simulations. Item (i) was discussed in Sec. III. Item (ii) becomes problematic when simulating low Ca, materialized by a noisy velocity field and an unphysical droplet behavior. The first practical problem relating to item (ii) is LB's lack of Galilean invariance or the "pinning" of drops onto the underlying lattice in very slow flow. Lishchuk and co-workers' method uses an interface force density [see Eq. (6)] and should sum to zero for closed interfaces. However, it has been found that numerical derivatives [despite $O(2)$ accuracy] introduce an error, leading to the pinning. It is reduced by eliminating the small but finite total interface force on any one drop by adding its negative to the interface, uniformly distributed. Reduced spurious interfacial flow exposes another artefact of all CFD: velocity field checkerboarding. We exploit a slow time variation by averaging two successive simulation states, reducing checkerboarding to negligible levels but leaving the accuracy of the model's dynamics unaffected to $O(u^2)$ [17]. The above improvements lead to reduced pinning, checkerboarding and spurious flow; see Fig. 2.

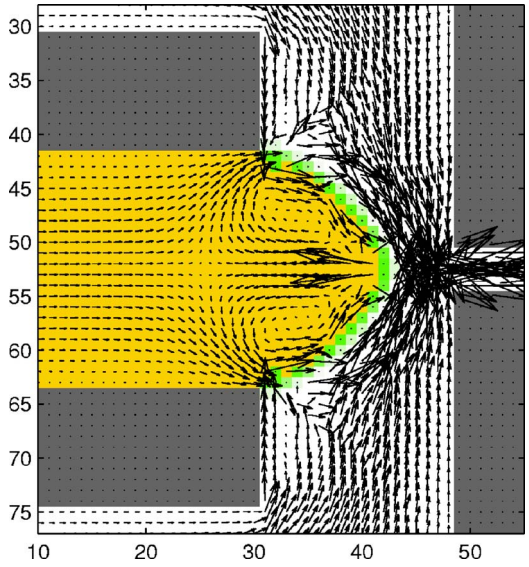

FIG. 3. (Color online) Drop formation and scission. Interimage interval is 1000 time steps. Simulation parameters were $\mathrm{Ca}=4\times10^{-4}$, $\mathrm{Re}=10^{-1}$. This time sequence is in good comparison with Ref. [1]. The surface wetting set at A makes the drop "stick" slightly.

V. RESULTS

Lattice dimensions were $L_x \times L_y = 160 \times 100$. The surface tension was calibrated by measuring the pressure increase across the interface of an isolated drop. Confirmed Laplace law behavior between a macroscopic surface tension α and the surface tension parameter σ ($R^2=0.985$, 30 points) was used to estimate Ca. The oil LBGK collision parameter varied from 0.2 to 1.5, depending on the Re. The oil influx, U_O, varied in 0.0015…0.011 lattice units per time step. Following [1], $U_W = U_O/4$. The measured increase in inlet pressure at steady state varied from 2% to 20%, depending on the Re.

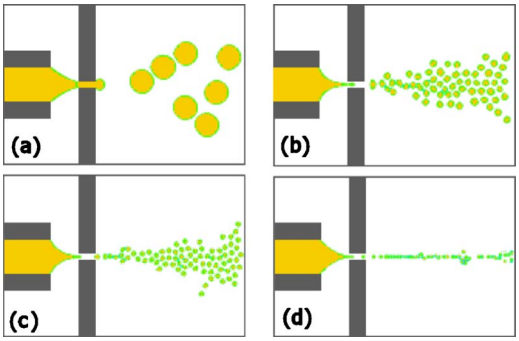

FIG. 4. (Color online) Steady state for {Ca, Re}: (a) (top left) $\{4\times10^{-4},0.10\}$, (b) (top right) $\{3\times10^{-3},0.62\}$, (c) (bottom left) {0.01, 2.7}, (d) (bottom right) {0.07, 17}. Wetting affinities and inlet velocity profiles are constant. (d) shows the effect of preferential supernatant wetting. Droplets size and distribution in the chambers are in good comparison with the images of Ref. [1].

The program execution required 5 (0.3) mins/droplet for the smallest (largest) Re on a UNIX Pentium 3.06 GHz and only 43 Mb of RAM. Re varied from 10^{-1} to 17; the corresponding Ca ranged from 3×10^{-4} to 6×10^{-2}. Generally, the model shows behavior very similar to the experiments of [1], as the time sequence of Fig. 3 shows. The latter depicts the formation of drops for Re=0.1, Ca=3×10^{-4} [parameters of Fig. 4(a)].

Our model is stable over a range of Re and Ca. Figure 4 shows the "steady-state" drop product distribution over 2 orders of magnitude of Ca and Re. The viscosity contrast and fluids' wetting affinities were constant in this data. There is a very clear variation in drop radius with Re, but for given Re, monodispersity is high, [1]. The third (unmodeled) dimension appeared to affect trends in comparison to the results of Anna *et al.*, especially at the aperture. Note also that our simulations show drop scission both within orifice A and downstream of it.

Sensitivity of our results to grid resolution was assessed by repeating the results of Fig. 4(a) with a range of increased resolutions. Average drop size was observed to remain constant for (up to) a factor of 10 (100) increase in the linear (area) density of mesh points.

As in all CFD models, the artifact of spurious velocities impacts in LB at low Ca. However, Fig. 2 shows that, in the most demanding regime (lowest Ca), our model achieves a very low spurious flow velocity field. Overall, it is clearly a great advantage that computational requirements scale only weakly with the number of drops.

VI. CONCLUSION

We report an efficient simulation of multicomponent microfluidics. Using a flow-focusing device (Fig. 1) as a test case, we used a two-dimensional multicomponent lattice Boltzmann method to simulate this low Ca, low Re, complex and unsteady flow in the continuum approximation over 2 orders of magnitude in Ca and Re (Fig. 4). Key developments of our model relate to control of spurious flow and treatment interfaces at the solid boundary, living an essentially clean velocity field (Fig. 2). Qualitative agreement with experiment [1] is good (Fig. 3).

A three-dimensional model of this system would bring only restricted benefits; while it would address a reported flow resistance of the drops (probably due to wetting on unmodeled boundaries), the latter could also be modeled in 2D, using an appropriate body force. For *effective* improvement we suggest (i) improving boundary conditions on the flow (phase field) by $O(2)$ accurate closure (dynamic wetting using a slip length) and (ii) further attention to drop pinning, using a distributed interface. Item (ii) is central to improving access to reduced Re but "costs" in terms of length scales.

ACKNOWLEDGMENTS

We acknowledge Dr. Chris Carey of Fluent Europe Ltd., and Dr. Chenghai Sun of the Steele Laboratory, Massachusetts General Hospital and Harvard Medical School for very helpful discussions.

[1] S. L. Anna, N. Bontoux, and H. Stone, Appl. Phys. Lett. **87**, 364 (2003).
[2] A. M. Gañán-Calvo and J. M. Gordillo, Phys. Rev. Lett. **87**, 274501 (2001).
[3] R. Benzi, S. Succi, and M. Vergassola, Phys. Rep. **222**, 145 (1992).
[4] S. Chen and G. D. Doolen, Annu. Rev. Fluid Mech. **30**, 329 (1998).
[5] S. Succi, *The Lattice Boltzmann Equation for Fluid Mechanics and Beyond* (Oxford-Clarendon, Oxford, 2001).
[6] M. M. Dupin, I. Halliday, and C. M. Care, J. Phys. A **36**, 8517 (2003).
[7] S. V. Lishchuk, C. M. Care, and I. Halliday, Phys. Rev. E **67**, 036701 (2003).
[8] M. M. Dupin, I. Halliday, and C. M. Care, Philos. Trans. R. Soc. London, Ser. A **362**, 1885 (2004).
[9] B. Li and Y. Kwok, Phys. Rev. Lett. **90**, 124502 (2003).
[10] L. S. Luo, Phys. Rev. Lett. **92**, 139401 (2004).
[11] S. Ansumali, C. E. Frouzakis, I. V. Karlin, and K. B. Boulouchos, Physica A **359**, 289 (2006).
[12] B. Li and D. Y. Kwok, Phys. Rev. Lett. **92**, 139402 (2004).
[13] R. Benzi, L. Biferale, M. Sbragaglia, S. Succi, and F. Toschi, J. Fluid Mech. **548**, 257 (2006).
[14] M. R. Swift, W. R. Osborn, and J. M. Yeomans, Phys. Rev. Lett. **75**, 830 (1995).
[15] A. K. Gunstensen, D. H. Rothman, S. Zaleski, and G. Zanetti, Phys. Rev. A **43**, 4320 (1991).
[16] O. Kuksenok, J. M. Yeomans, and A. C. Balazs, Phys. Rev. E **65**, 031502 (2002).
[17] M. M. Dupin, Ph.D. thesis, Sheffield Hallam University (2004).
[18] Y. H. Qian, D. d'Humieres, and P. Lallemand, Europhys. Lett. **17**, 479 (1992).
[19] T. Qian, X. P. Wang, and P. Sheng, Phys. Rev. E **68**, 016306 (2003).
[20] X. He and L.-S. Luo, J. Stat. Phys. **88**, 927 (1997).